Two-Stage Control for Small-Signal Modeling and Power Conditioning of Grid-Connected Quasi-Z-Source Inverter with LCL Filter for Photovoltaic Generation

F. Aalizadeh¹, M. Hosseinpour¹,², *, A. Dejamkhooy¹, H. Shayeghi¹,²

¹Department of Electrical and Computer Engineering, University of Mohaghegh Ardabili, Ardabil, Iran.
²Energy Management Research Center, University of Mohaghegh Ardabili, Ardabil, Iran.

Abstract- *Grid-connected inverter-based photovoltaic (PV) systems play an important role in Distributed Power Generation (DPG). For this application, quasi impedance source inverter is very suitable due to its ability to increase or decrease the output voltage of the inverter in a single-stage and high reliable condition. Conventionally, to remove the harmonics, which are yielded by switching the grid-connected inverter, LCL filters are utilized at the inverter output. These filters can cause some problems at the Point of Common Coupling (PCC). The aim of this paper is to improve the quality of the injected power of the photovoltaic array, which is connected to the low voltage grid by quasi-Z-source inverter (QZSI). For this purpose, a two-stage control procedure containing DC and AC stages is performed. In the DC stage, the dynamic characteristics of the quasi-Z-source network are investigated by small-signal analysis. Using the transfer functions obtained from the dynamic model, the capacitor voltage of the quasi-Z-source network is suitably controlled to generate the appropriate voltage to the grid interface inverter. In the AC stage, in order to inject high-quality current into the grid as well as eliminating the resonance peak caused by the LCL filter, a systematic procedure is used to design the PR controller parameters and active damping coefficient. Simulation of the overall system includes solar panels, maximum power point tracking algorithm, quasi-Z-source inverter, and LCL filter to model the grid-tied PV system with the possible details. Simulations are carried out in MATLAB/Simulink environment, and results depict suitable performance of the studied power conditioning system with designed parameters.*

Keyword: LCL filter, PR controller, Quasi-Z-source inverter, Small-signal modeling, THD.

1. INTRODUCTION

In recent years, fuel prices fluctuations have become a vital issue. In this regard, Renewable Energy Sources (RES), especially solar energy, have attracted much attention [1]. Solar energy is an effective way to compensate for the continuous increase in energy demand. However, there are some challenges in solar energy systems such as cost, size, and increasing output power. The V-I curve is characterized by a nonlinear PV array dependent on the solar radiation and temperature. In addition, in a given environmental condition, there is only one maximum power point in the PV array. Therefore, a controller is required for MPPT performance [2]. To convert power from renewable energy sources to the grid, using a Voltage Source

Inverter (VSI) or Current Source Inverter (CSI) is not enough. It is also necessary to use a DC / DC converter between the PV and the inverter to increase/decrease the PV voltage to obtain maximum power. In two-stage PV inverters, the complexity of the power and control circuit increases the cost and volume of the system and limits the efficiency. To eliminate the mentioned problems, single-stage converters have been introduced to connect PV arrays to the grid. Their advantages are compactness, low cost and high reliability [2-4]. The various impedance source based single-stage inverters are suitable solutions for converting PV array power to the grid. The Z-source inverter has a discrete input current which causes high stress capacitor voltage and converter control complexity. To improve conventional ZSI, QZSI has been introduced. Due to its continuous input current, it needs a smaller capacitor and less switching ripple [3].

According to IEEE std 1547, an appropriate filter is required to have standard harmonics at the inverter output [5]. Among different types of filters, LCL filters have better performance, less complexity, lower

inductance, and higher power density in comparing between L and LC filters [6-7]. A drawback, which limits the LCL filter, is the resonance phenomenon. It can cause instability problems [8]. Therefore, the intense effects of the LCL filter should be attenuated by damping methods where categorized into passive and active methods [9]. In the passive damping method, some resistors have utilized in series or parallel with the filter inductor or capacitor [10]. Active damping methods have received more attention due to their flexibility and lower power losses. However, the complexity of control and the cost of sensors has increased [11]. Two important types of active damping are single-loop and multi-loop methods. Multi-loop active damping method includes virtual resistance method [12], capacitor current feedback [13], capacitor voltage feedback [14] and grid current feedback [15]. Capacitor current feedback is the most famous damping method due to its efficiency, simple implementation and wide application [16].

In order to design a proper closed-loop control and achive to a stable performance of the converter, utilizing small-signal modeling is obvious [17]. The small-signal modeling methods, which have been mentioned in various articles, are average state space [18], PWM switch, signal flow-graph and energy factor [17]. An accurate QZSI model has been presented by small-signal analysis using the average state space method [18]. In this model, based on the dynamic model, the applications of the island and grid-connected modes have been implemented with an LC filter for a three-phase system with closed-loop control methods. To prevent the overlap between modulation index (M) and shoot-through duty cycle (d0), the QZSI capacitor voltage is controlled using transfer functions obtained by small-signal analysis. To ensure the stable operation of the system, the DC stage is controlled by two PI controllers to adjust the shoot-through duty cycle and capacitor voltage control using small-signal analysis. However, the AC stage is controlled by only a P controller for grid current regulation without any systematic design procedure. DC side control adjusts the capacitor voltage by controlling d0 where AC side control sets M for DC-AC converter. Then, both d0 and M control signals produce the appropriate switching signal through the PWM switching pattern. The small-signal analysis for conventional two-stage inverter and QZSI-based single-stage inverter in island mode with LC filter has been performed in Ref. [19] by the average mode space method. Then, the two-stage AC and DC controls for these two structures is investigated. In Ref.

[20], the small-signal model of QZSI with battery is presented. A control solution for the three-phase grid-connected PV system with an LC filter is given. For this aim, the spatial vector modulation method is used for switching the inverter. A QZSI-based PV system connected to a single-phase grid with an L filter is presented in Ref. [4]. A control structure consisting of two control loops with PI and PIS (sinusoidal PI) controllers is introduced. It should be noted that the DC and AC side controllers have not tuned by a systematic design procedure.

In Ref. [5], the PV array-based power conditioning system by using Trans-Z-Source single-stage inverter with an LCL filter is presented. Also, a systematic method for controlling grid current and eliminating the resonant frequency caused by LCL filter with active damping method is introduced. It is conducted by designing proportional-resonant controller parameters and capacitor current feedback coefficient that reduces the grid current THD. However, no solution is provided to control the DC side and capacitor voltage control of AC side controller and trial and error is used for this purpose. It is worth noting that the structure of the Trans-Z-Source inverter has a discrete input current, while it is often used with continuous input structures in PV applications. In Ref. [21], the PV array-based power quality improvement system is presented, which it is utilized grid-connected quasi-Y-source inverter with LCL filter. A step-by-step method is applied to design the AC side controller coefficients. The method is based on the control of the inductor current side of the converter, which has the inherent damping property for the LCL filter. Despite the precise design for the AC side controllers, the DC side control is not considered. In Ref. [22], the authors have presented the design of the LCL filter for the precise performance of the Modified Y-source inverter. So, the converter side control has a robust performance for the inverter filter based on the LCL filter. The presented structure is used to harvest power from the PV array. The focus is on AC side control and nothing has been done in the field of DC side control. In Refs. [23,24], PV power quality improvement system based on grid-connected voltage source inverter with LCL filter and Trans-Z-Source inverter with L filter is presented, respectively. The mathematical method has been used to design the PI and PR control coefficients of the AC side controllers, respectively. Despite the precise design for the AC side controller, the DC side control has not been considered and the trial and error method has been used to control the capacitor voltage with the PI controller on the AC

side. In Ref. [25], a grid-connected inverter with an L filter is provided, which uses the state feedback control method to control the AC side, but no solution is provided for the DC side. According to reviewed papers, some researches have provided precise control for the DC side by modeling the small-signal. However, they have not used the LCL filter with high injection current quality for the AC side. Other references have considered the LCL filter with a controller design for the AC side. However, they have not provided a precise control solution for the DC side. In this paper, the accurate model of the single-phase grid-connected QZSI with LCL filter is presented. Moreover, MPPT for a PV system is provided by the incremental inductance method. DC side dynamic characteristics of the quasi-Z-source inverter are investigated by small-signal analysis. Then, suitable transfer functions are extracted for the systematic design of PI controller coefficients in the closed-loop control of the DC side as well as capacitor voltage control of the AC side. Also, to control the AC side of the grid-connected quasi-Z-source inverter, a systematic method is used to design the PR controller coefficients as well as the capacitor current feedback active damping coefficient. The main innovation of this paper is the utilization of the small-signal analysis to drive the required transfer functions in the design of DC side and capacitor voltage control of AC side controller coefficients and its integration into injection current controller and the active damping of LCL filter in AC side control.

The structure of the paper is as follows: In Section 2, dynamic modeling of QZSI is presented with the small-signal method. Two-stage control method is examined in Section 3. Section 4 discusses controller design and active damping. Furthermore, Section 5 presents the simulation results and provides a comprehensive comparison between the results of the proposed system and similar research. Finally, in Section 6, the conclusion of the article is presented.

2. DYNAMIC MODELING OF A QUASI-Z-SOURCE NETWORK

2.1. Small-signal modeling of a quasi-Z-source network

For modeling the DC side of the QZSI, small-signal analysis is presented with details. The small-signal model of the QZSI is obtained by the average state-space method. The state space model includes the average of the equations of different states of the switches. The general QZSI circuit is shown in Fig. 1. In general analysis, the input voltage of v_{in} is considered the input of the system, which depends on the input

current of i_{in}. The reason is that renewable sources do not have output characteristics such as a voltage source or an ideal current source. For DC side modeling, the H-bridge module is equivalent to a switch and a current source with a parallel connection as an AC output load. In shoot-through mode, the switches of at least one leg of the H-bridge module are in ON state and the AC load terminals are shortened together. Therefore, the equivalent switch is ON and the QZSI equivalent circuit in the shoot-through mode is shown in Fig. 2-a. For non-shoot-through modes (six active modes and two conventional zero modes where all up or down switches are on), the equivalent switch is OFF and the QZSI equivalent circuit is shown in Fig. 2-b.

Considering the asymmetric quasi-Z-source network, four state variables can be defined including the current of the two inductors i_{L1}, i_{L2}, and the capacitors voltage v_{C1}, v_{C2}. The load current i_{Load} is considered as the input variable and v_{C1}, i_{L1} are considered as the output variables of the system. For simplification, it should be considered that $L = L_1 = L_2$, $C = C_1 = C_2$. Also, the series resistance of the inductors are equal as $r = r_1 = r_2$, and the series resistance of the capacitors are equal $R = R_1 = R_2$. If the shoot-through mode time interval is T_0, and the non-shoot-through interval is T_1, then the switching period will be $T_s = T_0 + T_1$. Therefore, the ratio of the shoot-through period is $d_0 = T_0/T_s$. In the shoot-through mode (Fig. 2-a), the capacitors convert their electrostatic energy into magnetic energy stored in the inductors.
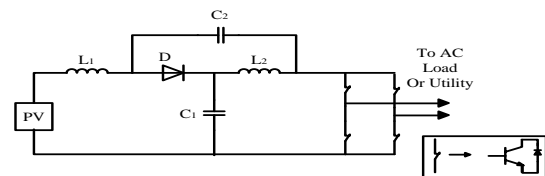

Fig. 1. Quasi-Z-source inverter for PV applications

(a)

(b)
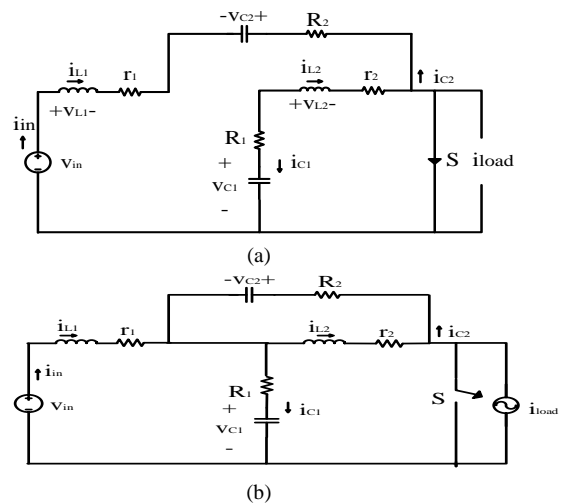
Fig. 2. The equivalent circuit for quasi-Z-source inverter equivalent: a. Shoot-through state, b. Non-shoot-through state
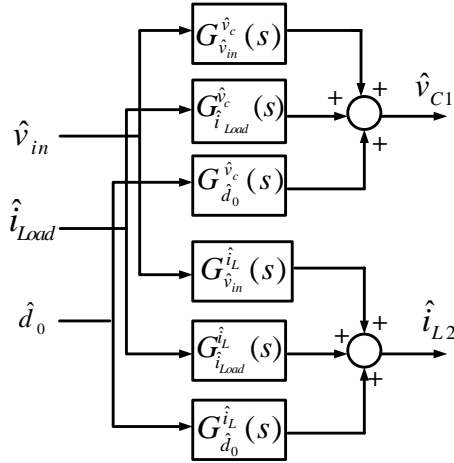
Fig. 3. Small-signal model for the quasi-Z-source network

The dynamic state equations of the quasi-Z-source network are given as follows [18]:

$$\frac{dx}{dt} = A_1 x + B_1 u \quad , \quad x = \begin{bmatrix} i_{L1} & i_{L2} & v_{C1} & v_{C2} \end{bmatrix}$$

$$A_1 = \begin{bmatrix} \dfrac{-(r+R)}{L} & 0 & 0 & \dfrac{1}{L} \\ 0 & \dfrac{-(r+R)}{L} & \dfrac{1}{L} & 0 \\ 0 & \dfrac{-1}{C} & 0 & 0 \\ \dfrac{-1}{C} & 0 & 0 & 0 \end{bmatrix} \quad (1)$$

$$B_1 = \begin{bmatrix} 0 & 0 & 0 & 0 \\ \dfrac{1}{L} & 0 & 0 & 0 \end{bmatrix}' \quad , \quad u = \begin{bmatrix} i_{Load} & v_{in} \end{bmatrix}$$

In the non-shoot-through mode (Fig.2-b), the DC power source, as well as inductors, charge capacitors and the external AC load which results in boosting the DC voltage across the inverter bridge. Dynamic state equations are shown by Eq. (2):

$$\frac{dx}{dt} = A_2 x + B_2 u$$

$$A_2 = \begin{bmatrix} \dfrac{-(r+R)}{L} & 0 & \dfrac{-1}{L} & 0 \\ 0 & \dfrac{-(r+R)}{L} & 0 & \dfrac{-1}{L} \\ \dfrac{1}{C} & 0 & 0 & 0 \\ 0 & \dfrac{1}{C} & 0 & 0 \end{bmatrix} \quad (2)$$

$$B_2 = \begin{bmatrix} \dfrac{R}{L} & \dfrac{R}{L} & \dfrac{-1}{C} & \dfrac{-1}{C} \\ \dfrac{1}{L} & 0 & 0 & 0 \end{bmatrix}^T$$

Using the state space equivalent, the DC side model

in QZSI can be obtained as Eq. (3). To obtain the small-signal model, perturbations $\hat{d}_0$, $\hat{v}_{in}$, $\hat{i}_{Load}$ are introduced with d_0, v_{in}, and i_{Load}, which in turn cause the creation of variables $\hat{i}_{L2}$, $\hat{v}_{C1}$, $\hat{v}_{C1}$, $\hat{v}_{C2}$ in the dynamic state variables of i_{L1}, i_{L2}, v_{C1}, v_{C2}, respectively. Substituting $x = \hat{x} + X$ that X and $\hat{x}$ represent the DC terms and the perturbations of the variables d_0, v_{in}, i_{Load}, i_{L1}, i_{L2}, v_{C1}, v_{C2}, in equation (3). Considering the inductors volt-second equilibrium, and capacitor charge balance in the stable mode and ignoring the second-order elements, the Laplace transform equations of the multi-input-multi-output quasi-Z-source network are obtained. The small-signal model of the quasi-Z-source network is shown in Fig. 3. The small-signal transfer functions can be achieved by considering two unrelated inputs to be zero. So, the small-signal transfer functions from the remaining input to the state variables are determined.

$$\frac{dx}{dt} = Ax + Bu \quad , \quad y = Cx + Du$$
$$A = d_0 A_1 + (1 - d0) A_2 \quad , \quad B = d_0 B_1 + (1 - d_0) B_2$$
$$y = \begin{bmatrix} v_{C1} \\ i_{L1} \end{bmatrix} \quad (3)$$
$$C = \begin{bmatrix} 0 & 0 & 1 & 0 \\ 1 & 0 & 0 & 0 \end{bmatrix} \quad , \quad D = \begin{bmatrix} 0 \\ 0 \end{bmatrix}$$

2.2. Dynamic characteristics of the quasi-Z-source network

Using the linearized state-space model, the converter transfer function can be calculated as follows:

$$G_{\hat{u}}^{\hat{y}}(s) = C.[sI - A]^{-1} B + D \quad (4)$$

According to the small-signal model, the transfer function from d_0 to capacitor voltage v_{C1} and v_{C2}, which are equal to $G_{\hat{d}_0}^{\hat{v}_c}$, is shown in Eq. (5). The transfer function from d_0 to inductor current i_{L1} and i_{L2}, which are equal to $G_{\hat{d}_0}^{\hat{i}_L}$ and the transfer function from i_{Load} to capacitor voltage v_{C1} and v_{C2}, which are equal to $G_{\hat{i}_{Load}}^{\hat{v}_c}$ are shown in Eqns. (6) and (7), respectively.

$$G_{\hat{d}_0}^{\hat{v}_c}(s) = \frac{\hat{v}_c(s)}{\hat{d}_0(s)} = \frac{(V_{C1} + V_{C2} - RI_{Load})(1 - 2D_0) + (I_{Load} - I_{L1} - I_{L2})(Ls + r + R)}{LCs^2 + C(R + r) + (1 - 2D_0)^2} \quad (5)$$
$$(\hat{i}_{Load}(s) = 0, \hat{v}_{in}(s) = 0)$$

$$G_{\hat{d}_0}^{\hat{i}_L}(s) = \frac{\hat{v}_c(s)}{\hat{d}_0(s)} = \frac{(V_{C1} + V_{C2} - RI_{Load})Cs - (I_{Load} - I_{L1} - I_{L2})(1 - 2D_0)}{LCs^2 + C(R + r) + (1 - 2D_0)^2} \quad (6)$$
$$(\hat{i}_{Load}(s) = 0, \hat{v}_{in}(s) = 0)$$

$$G_{\hat{i}_{Load}}^{\hat{v}_c}(s) = \frac{\hat{v}_c(s)}{\hat{i}_{Load}(s)} = \frac{R(1 - 2D_0)(1 - D_0) - (1 - D_0)(Ls + r + R)}{LCs^2 + C(R + r) + (1 - 2D_0)^2} \quad (7)$$
$$(\hat{v}_{in}(s) = 0, \hat{d}_0(s) = 0)$$

2.3. Capacitor voltage control

According to the operating principles of the qausi-Z-source inverter, d_0 or M can be increased to increase the voltage gain. However, d_0 and M are interdependent due to the single-stage structure. For this purpose, the the traditional zero modes of a conventional inverter can be replaced by the shoot-through modes in the quasi-Z-source inverter, and the remaining six active modes do not change. According to the simple boost method, the relationship between M and D_0 will be as follows:

$$M \leq 1 - D_0 \tag{8}$$

The symbol D_0 is used for the permanent state. By changing d_0 or M, other parameters will be affected. It makes the controller design harder. Therefore, using a large d_0 and a small value for M is not economical at the same voltage gain. This solution increases the voltage stress on the switches and increases the rating of the components and thus their price. The boost coefficient of the converter is also calculated as [5]:

$$B = \frac{1}{1 - 2D_0} \tag{9}$$

In the steady-state condition, the peak voltage of the inverter can be calculated as [18]:

$$V_{p-peak} = \frac{1}{2} \cdot \frac{V_{in}}{1 - 2D_0} M \tag{10}$$

The relationship between capacitor voltage and the input voltage is as:

$$V_{C1} = \frac{1 - D_0}{1 - 2D_0} V_{in} \tag{11}$$

$$V_{C2} = \frac{D_0}{1 - 2D_0} V_{in} \tag{12}$$

The relationship between inductor and load currents is Eq. (13). The capacitor voltage inequality is Eq. (14).

$$I_{L1} = I_{L2} = \frac{1 - D_0}{1 - 2D_0} I_{Load} \tag{13}$$

$$V_{C1} \geq 2V_{p-peak} \tag{14}$$

Equation (14) can easily keep the capacitor C_1 voltage almost more than twice the output peak voltage to prevent the intersection of M and d_0. Since in most applications of distributed generation, where the capacitor voltage may be controlled at a constant value with variable input, V_{p-peak} is kept constant. In a closed-loop control, the capacitor voltage can be kept to a minimum value considering equation (14). As a result, the minimum value of D_0 and the maximum value of M are achieved, which means that there will be lower voltage stress on the switches. In distributed generation for grid-connected applications, the QZSI should operate as a current source and inject an appropriate current to the grid where its output voltage is forced by the grid voltage. The next section will discuss the controller design for both AC and DC parts.

3. TWO-STAGE CONTROL METHOD FOR LCL FILTERED GRID-CONNECTED QZSI

There are two important control features for PV-based QZSIs: 1) Satisfactory power quality, output voltage/current with desirable amplitude and frequency, and limited THD. 2) Adequate voltage increase to achieve the desired AC voltage level. To maximize solar energy harvesting, MPPT system is essential. Also, a PV voltage regulator should be employed to track time-varying reference voltages. The V_{MPP} value is continuously tracked by specific MPPT algorithms. In two-stage PV systems, the DC-DC converter and the voltage source inverter are decoupled by a DC link capacitor. This capacitor plays an important role in determining the power balance between the input and output side of the PV system. The capacitor voltage should be kept constant. This method is also used for the QZSI system in which the capacitor in the quasi-Z-source network acts like a decoupled capacitor. In this work, the capacitor C_1 of the quasi-Z-source network acts as a decoupled capacitor. Fig. 4 displays the general configuration of the QZSI system for connecting the PV array to the grid by an LCL filter, in which L_{f1}, L_{f2}, C_f are the inductors and capacitor of LCL filter. Also, i_{Cf}, i_{Lf}, i_g are the filter capacitor current, the inductor filter current and the grid current, respectively. In the following, the design of the controller for controlling the DC side as well as the AC side of the grid-connected inverter with LCL filter will be discussed.

3.1. Controller design for DC side

After decoupling by the capacitor, the DC and AC side controls are considered separately as in Fig. 5. Generated pulses by DC side controller (to increase voltage) and AC side controller (for DC-AC conversion) using an OR logic gate is integrated. The intersection of M and d_0 is avoided by adjusting the reference voltage of the capacitor based on Equation (14). DC side control can be accomplished in two methods illustrated in Fig. 5, where one of these methods will be employed to generate the shoot-through signals. In the first method, The v_{C1} dynamics generated by d_0 are obtained by the transfer function based on Equation (4) is compared with the reference voltage of capacitor $v_{C1,ref}$ and the error goes through a PI controller to set d_0. The d_0 feed-forward PI controller is used as a shoot-through compensator using a linear approximation. d_0 is determined by the relation between v_{C1}, v'_{in}, in the permanent state according to Eq. (15).
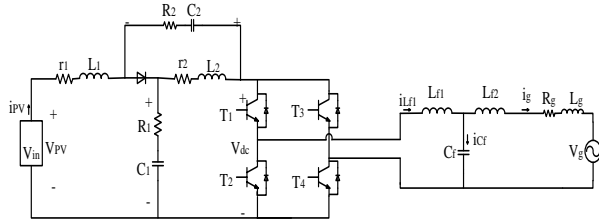
Fig. 4. Investigated QZSI configuration for the grid connection of PV Arrays
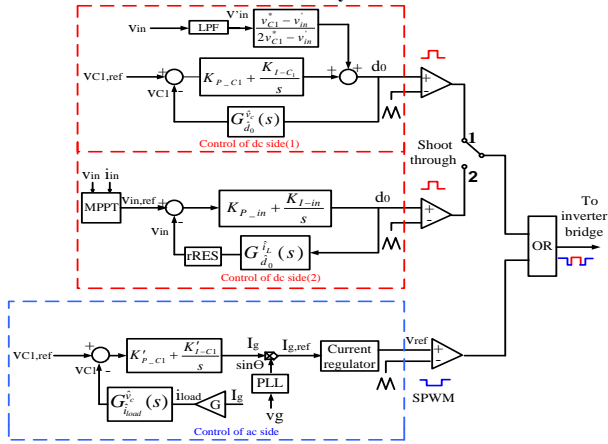
Fig. 5. Two-stage control for grid-connected QZSI
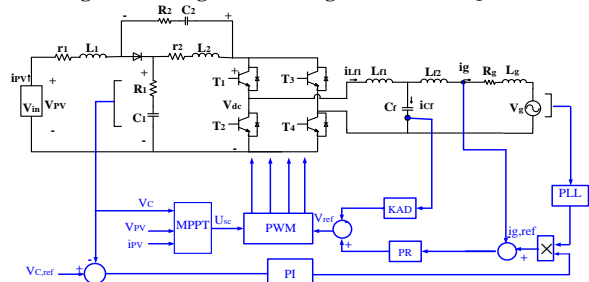
**Fig. 6. The Overall control scheme for PV based grid-connected QZSI**
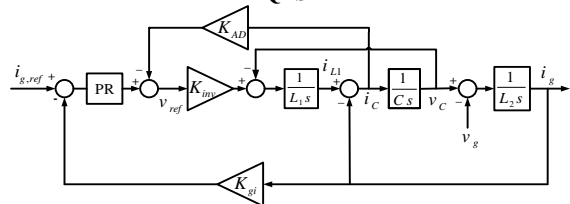
Fig. 7. Control block diagram for PR controller and active damping

$$d_0 = \left[\frac{v_{C1,ref} - v'_{in}}{2v_{C1,ref} - v'_{in}} \right] \tag{15}$$

where v'_{in} is a low ripple input voltage which is obtained by passing the input voltage v_{in} through a low-pass filter. Using small-signal modeling, the PI parameters for the v_{C1} control loop can be determined. To prevent the DC and AC side dynamics from adversely affecting each other, the DC side dynamics must be much slower, which can be achieved by having a lower bandwidth in the DC side voltage loop. In the second method, the value of the input reference voltage $V_{in,ref}$ of the PV system is obtained from the MPPT

algorithm. Using the transfer function according to Equation (6) and r_{RES} which convert input current to the input voltage, the result of subtracting two signals is applied to a PI controller to create d_0. The PI controller is used to set d_0. The DC side PI parameters are selected compared to the V_{C1} control loop to ensure a slower response system performance. In capacitor voltage control, as long as V_{C1} is held constant by the DC side controller, the input reference voltage tracking is achieved by setting d_0 on the DC side in the steady-state according to Equation (15). The input reference voltage $V_{in,ref}$ in QZSI is given by PV. By using the $G_{d_0}^{\hat{i}_L}$, the changes of d_0 will cause to change in the input current of i_{L1}, which can be converted to input voltage by r_{RES} impedance. The PI parameters for the V_{in} control loop are selected using small-signal modeling. To ensure the correct operation of the system, the DC side PI parameters are selected by comparing with the V_{C1} control loop with a relatively slower response.

3.2. Controller design for AC side

Control of injected power into the grid in a PV system is an important issue that should be discussed. DC link capacitor voltage is a good measure for determining the power flow. When this voltage rises above its reference value, the control system must reduce d_0 to ensure system stability. Fig. 6 demonstrates the outline of the studied system and the control scheme of the grid-connected PV system with a quasi-Z-source inverter. According to Fig. 6, the capacitor voltage of the QZSI network using $G_{\hat{i}_{load}}^{\hat{v}_c}$ according to Equation (7) is compared with the capacitor reference voltage. The error signal is then controlled with a PI controller to generate the reference current amplitude. A coefficient G is used to transfer I_g to i_{load}, which relates to inverter operating condition (e.g. modulation index, shoot-through duty ratio and the power factor). To achieve unity power factor injection, a Phase Locked Loop (PLL) block extracts the grid voltage phase and multiplies it by the output value of the PI controller. It also produces the reference current value ($i_{g, ref}$) to control the injected grid current. By subtracting the sampled grid current from $i_{g, ref}$, an error signal is given to a PR controller. An active damping method is used to ensure high-quality power injection. The design of the active damping coefficient parameter and PR controller is discussed in the next section.

3.2.1. Control of injected current to grid

By writing Kirchhoff's rules for the system, we will have [5]:
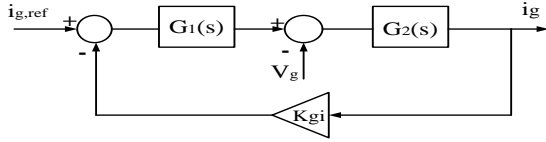
Fig. 8. Equivalent block diagram for control scheme
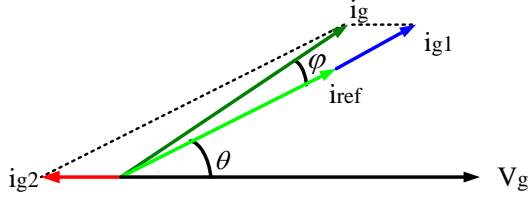
Fig. 9. Phasor diagram of grid voltage and injected current to grid

$$\begin{cases} L_1 \dfrac{di_1}{dt} = u_i - u_c \\[2mm] L_2 \dfrac{di_g}{dt} = u_c - u_g \\[2mm] C \dfrac{du_c}{dt} = i_c \\[2mm] i_1 = i_g + i_c \end{cases} \qquad (16)$$

The system block diagram is shown in Fig. 7. As can be seen, the difference between the actual injected current to the grid and the reference current is given to the PR controller. In order to compensate the filter resonance peak, filter capacitor current feedback has been added to these reference values. The error resulting from the comparison of the PR controller and the current feedback coefficient makes the reference voltage (v_{ref}) for the inverter. It should be noted that according to the Fig. 6, the shoot-through duty cycle resulting from the DC side control decreases from the unit value and makes the U_{sc} signal. Finally, these signals are used as inputs for the PWM switching block. The unipolar switching method is used for this application, which will eventually producing three-level voltage at the inverter output. The gain of the inverter is considered as K_{inv} in the Fig. 7. The design of control parameters and capacitor current feedback coefficient is explained in the following section.

4. DESIGN OF PR CONTROLLER AND ACTIVE DAMPING COEFFICIENT

4.1. Control scheme modeling

The illustrated diagram in Fig. 7 can be simplified as shown in Fig. 8, where $G_1(s)$, $G_2(s)$ and $G_{PR}(s)$ are as follows:

$$G_1(s) = \frac{K_{inv} G_{PR}(s)}{C L_{f1} s^2 + K_{inv} K_{AD} C_f s + 1} \qquad (17)$$

$$G_2(s) = \frac{C_f L_{f1} s^2 + K_{inv} K_{AD} C_f s + 1}{L_{f1} L_{f2} C_f s^3 + L_{f2} C_f K_{AD} K_{inv} s^2 + (L_{f1} + L_{f2}) s} \qquad (18)$$

$$G_{PR}(s) = K_P + \frac{2 K_r s}{s^2 + \omega_1^2} \qquad (19)$$

The ideal PR controller shown in (19) is indistinguishable due to component tolerance in analog systems and limited in digital systems accuracy [26, 27]. The transfer function of a non-ideal PR controller is given in Equation (20), where K_P and K_r are proportional gain and resonant gain and ω_{PRC} and ω_1 are the resonant frequency around the bandwidth and the main frequency, respectively. Non-ideal PR controllers are less sensitive to resonant frequency deviations than ideal controllers.

$$G_{PR}(s) = K_P + \frac{2 K_r \omega_{PRC} s}{s^2 + 2\omega_{PRC} s + w_1^2} \qquad (20)$$

K_{AD} is the active damping coefficient and $G_{PR\,(s)}$ is the transfer function of the PR controller. According to Fig. 8, the open-loop transfer function is calculated as:

$$T(s) = \frac{K_{gi} K_{AD} G_{PR}(s)}{L_{f1} L_{f2} C_f s^3 + L_{f2} C_f K_{AD} K_{inv} s^2 + (L_{f1} + L_{f2}) s} \qquad (21)$$

If the grid current is considered as the effects of reference current and grid voltage, it can be derived that:

$$i_g(s) = i_{g1}(s) + i_{g2}(s) \qquad (22)$$

$$\begin{cases} i_{g1}(s) = \dfrac{1}{K_{gi}} \dfrac{T(s)}{1 + T(s)} i_{ref}(s) \\[3mm] i_{g2}(s) = -\dfrac{G_2(s)}{1 + T(s)} V_g(s) \end{cases} \qquad (23)$$

According to Fig. 9, by considering the φ deviation angle between $i_{g1\,(s)}$ and $i_{g\,(s)}$, $\tan(\varphi)$ can be calculated:

$$\begin{aligned} \tan(\varphi) &= \left| \frac{i_{g2}(s)}{i_{g1}(s)} \right| = \left| \frac{K_{gi} G_2(s) V_g(s)}{T(s) i_{ref}(s)} \right|_{s=j\omega_1} \\[2mm] &= \left| \frac{K_{gi} G_2(j\omega_1)}{T(j\omega_1)} \frac{V_g(j\omega_1)}{i_{ref}(j\omega_1)} \right| \end{aligned} \qquad (24)$$

Assuming $s = j\omega_1$ in $G_{PR}(s)$, so:

$$\begin{aligned} G_{PR}(j\omega_1) &= K_P + \frac{2 K_r \omega_{PRC} j\omega_1}{(j\omega_1)^2 + 2\omega_{PRC} j\omega_1 + \omega_1^2} \\[2mm] &= K_P + K_r \end{aligned} \qquad (25)$$

The LCL filter capacitor value can be omitted by regarding to this fact the resonant frequency of the LCL filter is much higher than the main frequency:

$$\begin{cases} C_f = 0 \\[2mm] G_2(j\omega_1) = \dfrac{1}{(L_{f1} + L_{f2})(j\omega_1)} \end{cases} \qquad (26)$$

Therefore, it can be concluded in Eq. (27). V_g is the effective value of the grid voltage and I_{ref} is the effective value of the reference current. T_{f1} is the size of the open-loop transfer function in f_1 (fundamental frequency) in dB as Eq. (28). According to Fig. 8, the

E_A current error can be calculated as Eq. (29).

$$\begin{cases} \tan(\varphi) = \left| \dfrac{K_{gi}}{T(j\omega_1)(L_{f1}+L_{f2})(j\omega_1)} \right| \left| \dfrac{V_g(j\omega_1)}{i_{ref}(j\omega_1)} \right| \\ T(j\omega_1) = \dfrac{K_{gi}}{\tan(\varphi)(L_{f1}+L_{f2})(\omega_1)} \cdot \dfrac{V_g}{I_{ref}} \end{cases} \quad (27)$$

$$T_{f1} = 20\log|T(j\omega_1)| = 20\log\left(\frac{K_{gi}V_g}{\tan(\varphi)I_{ref}(L_{f1}+L_{f2})(\omega_1)}\right) \quad (28)$$

$$E_A = \frac{\left|K_{gi}i_g(j\omega_1)\right| - I_{ref}}{I_{ref}} = \frac{K_{gi}\left|i_{g1}(j\omega_1)\right|/\cos\varphi}{I_{ref}} - 1 \quad (29)$$

By inserting $i_{g1\ (s)}$ from Eqns. (23) - (29), E_A can be expressed as:

$$E_A = \left|\frac{T(j\omega_1)}{1+T(j\omega_1)}\right| \frac{1}{\cos\varphi} - 1 \quad (30)$$

If $T_{f1} \geq 40\text{dB}$, then $T(j\omega_1) \approx 1 + T(j\omega_1)$. Therefore (27) can be rewritten as follows:

$$E_A = \left|\frac{T(j\omega_1)}{1+T(j\omega_1)}\right| \frac{1}{\cos\varphi} - 1 \approx \frac{1}{\cos\varphi} - 1 \quad (31)$$

According to Eq. (31) and Fig. 9, to obtain the zero-error $\cos(\varphi)$ should be unit. It means $\varphi = 0$. As the reference current phase is defined by the PLL, $i_{ref\ (s)}$ and $V_{g\ (s)}$ have the same phase and $\theta = 0$.

4.2. Proportional-Resonant controller

4.2.1. Proportional gain (K_P)

The resonant frequency of the LCL filter is obtained as:

$$f_{res} = \frac{1}{2\pi}\sqrt{\frac{L_{f1}+L_{f2}}{L_{f1}L_{f2}C_f}} \quad (32)$$

The gain crossover frequency (f_c) is usually slightly lower than the switching frequency (f_{sw}). To prevent the effect of high-frequency noise attenuation, the resonant frequency of the LCL filter is limited in the range of $f_{sw}/2$ to $f_{sw}/4$. It removes the harmonics and operates with good dynamics [5]. To complete the design and proper operation of the grid-connected quasi-Z inverter with LCL filter, f_c is selected less than $f_{sw}/10$. Because f_c is about ten times smaller than f_{sw} and less than the resonant frequency of the LCL filter. The capacitor effect can be ignored [5]. Therefore, the open-loop transfer function of the system is obtained as:

$$|T(s)| \approx \left|\frac{K_{gi}K_{inv}G_{PR}(s)}{(L_{f1}+L_{f2})s}\right| \quad (33)$$

The PR controller equations can be simplified because the cut-off frequency is greater than the fundamental frequency, so that the PR controller resonance term can be ignored:

$$G_{PR}(j\omega_c) = K_P + K_r \approx K_P \quad (34)$$

Therefore, the open-loop transfer function can be rewritten as:

$$|T(j\omega_c)| \approx \left|\frac{K_{gi}K_{inv}K_P}{(L_{f1}+L_{f2})j\omega_c}\right| \quad (35)$$

The amplitude of system frequency response at the cut-off frequency is zero and this can be used to calculate the proportional gain:

$$20\log|G(j2\pi f_c)| \approx 20\log\left|\frac{K_{gi}K_{inv}K_P}{(L_{f1}+L_{f2})j\omega_c}\right| = 0 \quad (36)$$

$$K_P = \frac{2\pi f_c(L_{f1}+L_{f2})}{K_{gi}K_{inv}} \quad (37)$$

4.2.2. Resonant gain (K_r)

Considering the controller transfer function according to Eq. (20) in the fundamental frequency, the following equation is obtained:

$$G_{PR}(j\omega_1) = K_P + \frac{2K_r\omega_{PRC}(j\omega_1)}{(j\omega_1)^2 + 2\omega_{PRC}(j\omega_1) + \omega_1^2} \quad (38)$$
$$= K_P + K_r$$

According to Eqns. (33) and (37) it can be inferred that:

$$\left.|T(s)|\right|_{s=j\omega_1} \approx \left|\frac{K_{gi}K_{inv}(K_P + K_r)}{(L_{f1}+L_{f2})(j\omega_1)}\right| \quad (39)$$

Considering Eq. (28) we will have:

$$\begin{cases} T_{f1} = 20\log|T(j\omega_1)| \\ T_{f1} = 20\log\left|\dfrac{K_{gi}K_{inv}(K_P + K_r)}{(L_{f1}+L_{f2})(j\omega_1)}\right| \end{cases} \quad (40)$$

$$K_r = \frac{2\pi(L_{f1}+L_{f2})}{K_{gi}K_{inv}}(10^{\frac{T_{f1}}{20}}f_1 - f_c) \quad (41)$$

By placing $j\omega c$ in s in Eq. (20), the equation (42) is obtained:

$$G_{PR}(j\omega_c) = K_P + \frac{2K_r\omega_{PRC}(j\omega_c)}{(j\omega_c)^2 + 2\omega_{PRC}(j\omega_c) + \omega_1^2} \quad (42)$$

Since $(j\omega_c)^2 + 2\omega_{PRC}(j\omega_c)$ is much larger than ω_1^2, the term ω_1^2 can be ignored and $G_{PR\ (s)}$ will be obtained as:

$$G_{PR}(s) = K_P + \frac{2K_r\omega_{PRC}}{s} \quad (43)$$

Considering the optimal phase margin for the system to reach the PM value, it can be inferred that:

$$\pi + \angle T(j\omega_c) = PM \quad (44)$$

Using Eq. (21) with Eq. (41) and Eq. (42), K_r can be calculated according to Eq. (45).

$$K_r = \frac{(\frac{L_{f1}+L_{f2}}{L_{f2}C_f}) - 2\pi L_{f1}f_c^2 - K_{AD}K_{inv}f_c\tan(PM)}{K_{AD}K_{inv}f_c + ((\frac{L_{f1}+L_{f2}}{L_{f2}C_f}) - 2\pi L_{f1}f_c^2)\tan(PM)} \cdot \frac{\pi f_c K_P}{\omega_{PRC}} \quad (45)$$

4.2.3. Capacitor current feedback coefficient K_{AD}

By placing Eqns. (37) and (41) in Eq. (45), the K_{AD} is

calculated according to Eq. (46). The Gain Margin (GM) of the system at the resonant frequency is calculated according to Eq. (47) and by placing $j\omega_r$ for s in Eq. (25) will give the equation of Eq. (48).

$$K_{AD} = \frac{(\frac{L_{f1}+L_{f2}}{L_{f2}C_f}) - 2\pi L_{f1}f_c^2}{K_{inv}f_c} \times \frac{\pi f_c^2 - (10^{\frac{T_{f1}}{20}}f_1 - f_c)\omega_{PRC}\tan(PM)}{(10^{\frac{T_{f1}}{20}}f_1 - f_c)\omega_{PRC} + \pi f_c^2 \tan(PM)} \quad (46)$$

$$GM = -20\log|T(j\omega_r)| \quad (47)$$

$$G_{PR}(j\omega_r) = \left| K_P + \frac{2K_r\omega_{PRC}(j\omega_r)}{(j\omega_r)^2 + 2\omega_{PRC}(j\omega_r) + \omega_1^2} \right| \quad (48)$$

Since the denominator, which contains K_r, is much larger than the numerator, this part can be ignored and Eq. (49) rewritten as:

$$|G_{PR}(j\omega_r)| = K_P \quad (49)$$

By placing Eqs. (37) and (49) in Eq. (21) at $j\omega_r = s$, $T(j\omega_r)$ can be expressed as Eqs. (50) and (51). Since $(K_{AD}K_{inv})^2$ is much larger than $4\omega_r^2 L_{f1}^2$, the last part can be ignored in Eq. (49), so $T(j\omega_r)$ is simplified as:

$$T(j\omega_r) = \frac{A}{B} = \frac{2\pi f_c(L_{f1}+L_{f2})}{-(\omega_r)^2(L_2C_f K_{AD}K_{inv}) - j\omega_r(L_{f1}L_{f2}C_f\omega_r^2 + (L_{f1}+L_{f2}))} \quad (50)$$

$$\begin{cases} |A| = 2\pi f_c(L_{f1}+L_{f2}) \\ |B| = \frac{L_{f1}+L_{f2}}{L_{f1}}\sqrt{(K_{AD}K_{inv})^2 + 4\omega_r^2 L_{f1}^2} \end{cases} \quad (51)$$

$$|T(j\omega_r)| = \frac{|A|}{|B|} = \frac{2\pi f_c L_{f1}}{K_{AD}K_{inv}} \quad (52)$$

Considering Eqns. (47) and (52), the minimum value of K_{AD} is expressed by Equation (53).

$$K_{AD} = 10^{\frac{GM}{20}} \cdot \frac{2\pi f_c L_{f1}}{K_{inv}} \quad (53)$$

Table 1. PV array parameters at 25º C and 1000 W/m²

Parameter	Value
I_{mp}	30.44 A
V_{mp}	78.9 V
P_{max}	3075 W
I_{sc}	32.84 A
V_{oc}	98.7 V
N_s	3
N_p	5

Table 2. System parameters

Parameters	Values
L	1.5 mH
C	3000 µF
$r_l = r_{RES}$	0.25 Ω
r_c	0.03 Ω
D	0.35
V_s	110 V
f	60 Hz
f_{sw}	10 KHz
ω_i	10 rad/s
ω_1	2*pi*60
L_{1f}	1000 µF
C_f	20 µF
L_{2f}	0.25 mH
Rg	0.01 Ω
Lg	175 pH

4.2.4. Design considerations

The size of the open-loop transfer function at the fundamental frequency (T_{f1}) is the starting point for designing the controller parameters. As mentioned in Eq. (31), T_{f1} must be greater than 40 dB. In this paper, T_{f1} is considered to be 45 dB. After calculating K_P and defining T_{f1}, the next step is to calculate the minimum resonant gain K_r with equation (41). The upper bound of the K_{AD} is obtained using Eq. (46). The lower bound of K_{AD} preferably depends on the GM and the cut-off frequency of the system's main parameters. Using EQ. (53) and considering $GM = 5dB$ in the resonant frequency, the minimum value of K_{AD} is obtained. Once the K_{AD} range is defined and the appropriate value for the K_{AD} is selected. The upper bound of K_r is calculated using Eq. (45). It can be noted that as the amount of K_{AD} decreases, the phase margin of the open-loop system increases. To choose a suitable value for K_r, it should be taken into account that greater K_r leads to smaller GM.

5. SIMULATION RESULTS

The solar array parameters and the LCL filter parameters are presented in Table 1 and Table 2. Since the filter resonant frequency must be in the range of $f_{sw}/2$ to $f_{sw}/4$, the resonant frequency is selected 2516 Hz. For proper operation of single-phase grid-connected quasi-Z inverter with LCL filter, f_c should be selected a value less than $f_{sw}/10$ [5]. So, the cut-off frequency is set to 630 Hz. K_p proportional gain is designed equally to 0.7265 using Eq. (37). the lower limit of the K_r resonance gain is selected 11 by Using Eq. (40). The upper bound is selected equal to 0.3 for the active damping coefficient of K_{AD} using Eq. (46). According to Equation (53), the lower bound of K_{AD} will be 0.041. To achieve the appropriate phase margin for the system, K_{AD} has been selected 0.045. After the definition of K_{AD}, the upper range of the K_r resonance coefficient is in the range of 11 to 130. Considering the appropriate phase margin and the appropriate gain margin, K_r is set to about half of the maximum values and equal to 60. Also, coefficient K_{gi} is equal to 0.04.

Fig. 10 displays the open-loop diagram of the system. As can be seen, using the designed parameters, the phase margin will be 61.3º and the gain margin will be 3.5 dB, which is a good value for a controlled system. As shown in Fig. 11-a, by using the MPPT method, the PV array has a 90% efficiency. The harvested power from PV arrays is 2740 W where the rated power of PV arrays is 3075 W. One of the main goals of the control system is to inject power in full agreement with grid standards. According this aim, the sinusoidal injected current into the grid is shown in Fig. 11-b.
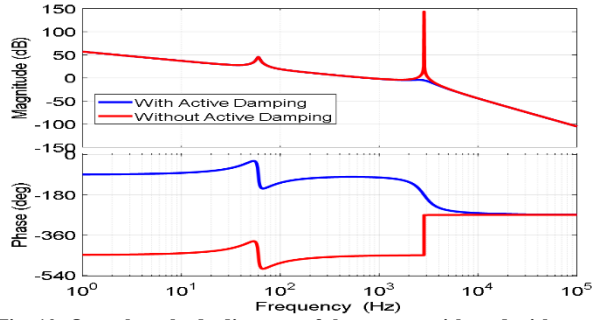
Fig. 10. Open-loop bode diagram of the system with and without active damping
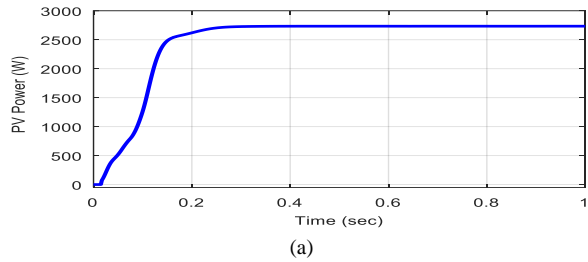
(a)
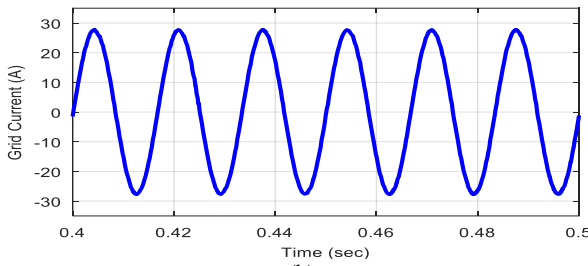
(b)

Fig. 11. a. Output power of PV arrays, b. injected current to grid
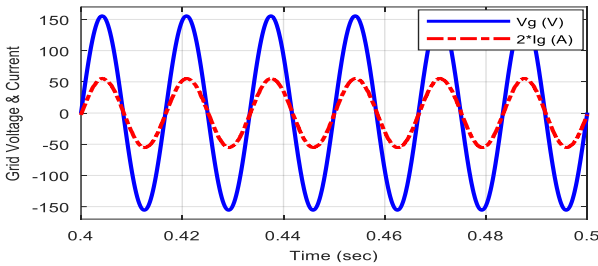
(a)
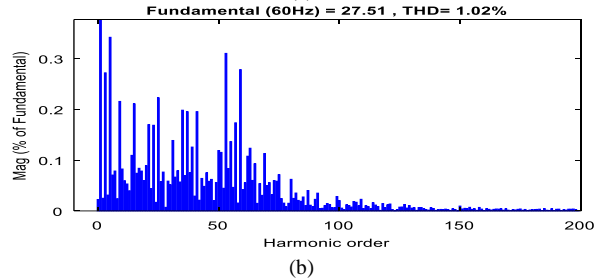
(b)

Fig. 12. a. Grid voltage and grid current, b. THD of grid current
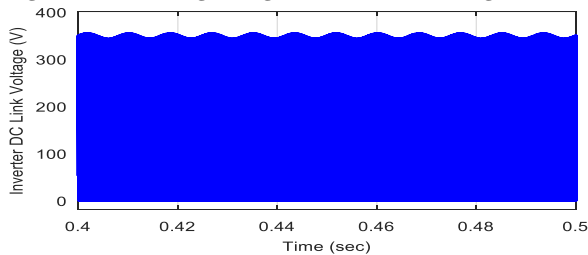
Fig. 13. Output voltage of QZSI as well as input voltage of the H-bridge module

Fig. 12-a simultaneously illustrates the grid voltage and current in steady-state condition. As can be seen, a sine wave current of 60 Hz is injected into the grid and there is no phase shift between the grid voltage and the current. Therefore, the power factor injected into the grid is equal to one. Fig. 12-b also demonstrates that the THD of the injected current, which is 1.01%. It is a very low and desirable value. It should be noted that the power efficiency of the grid-connected inverter is equal to 97%. Therefore, the efficiency of the total power conditioning system is 87.3% by considering the PV array and inverter, which is an acceptable value. Fig. 13 shows the output voltage of the quasi-Z network, which is considered as the input voltage of the H-bridge structure. In shoot-through intervals this voltage is equal to zero and in non-shoot-through intervals the voltage is about 345 V. The rapid changes between these two values due to high frequency switching value make this voltage appear solid. According to Equation (9), the boost coefficient of the quasi-Z network for the assumed modulation index as well as shoot-through duty cycle will be equal to 3.3, which corresponds to the amount of voltage in Fig 13. Fig.14-a displays the step response of the closed-loop transfer function of $G_{d_0}^{v_c}$ and Fig. 14-b demonstrates the bode diagram of the open-loop transfer function of $G_{d_0}^{v_c}$ before designing the PI controller. It deals with the first method of designing the DC side controller. The phase margin is equal to -84.4 ° and the gain margin is -38.1 dB. These values indicate system instability. Fig. 14-c also displays the step response and Fig.14-d illustrates the bode diagram of the system after PI controller design. With this design process, the phase margin is equal to 64.2º, the gain margin is 17.5 dB, the overshoot is equal to 1.17%, the rise time is equal to 0.0119 s and the settling time is 0.0543 s. The coefficients of K_{P_C1} and K_{I_C1} are selected as 0.001 and 0.08, respectively. As a result, the closed-loop system is stable and has a suitable dynamic behavior based on the obtained values. The figures of the step response and the bode diagram of the transfer function before and after designing the PI controller for the second method of DC side controller design are similar to first method. With this design process, the phase margin is 83º and the gain margin is inf, Overshoot is 6.49%, rise time is 5.16e-4 s and settling time is 0.003 s. The K_{P_in} and K_{I_in} coefficients are selected as 0.06 and 35.12, respectively. The closed-loop system is stable and has a good dynamic behavior. Fig. 15-a displays the step response of the closed-loop transfer function for $G_{\hat{i}_{load}}^{\hat{v}_c}$ and Fig.15-b shows the bode diagram of the open-loop

transfer function of $G^{\hat{v}_c}_{i_{load}}$ (capacitor voltage control of AC-side controller design) before designing the PI controller. The phase margin is equal to 92.4 ° and the gain margin is inf. Fig.15-c demonstrates the step response and Fig.15-d shows the bode diagram of the system after designing PI controller. By this design process, the gain margin is inf, the phase margin is 64.6 degrees, Overshoot is 7.19%, rise time is 0.0063 seconds and settling time is 0.0327 seconds. The K'_{P_C1} and K'_{I_C1} coefficients are selected as 0.37 and 70.2, respectively. Despite the stability of the bode diagram before designing, the step response has steady-state error and after designing the steady-state error disappears and the closed-loop system is stable and has a good dynamic behavior.
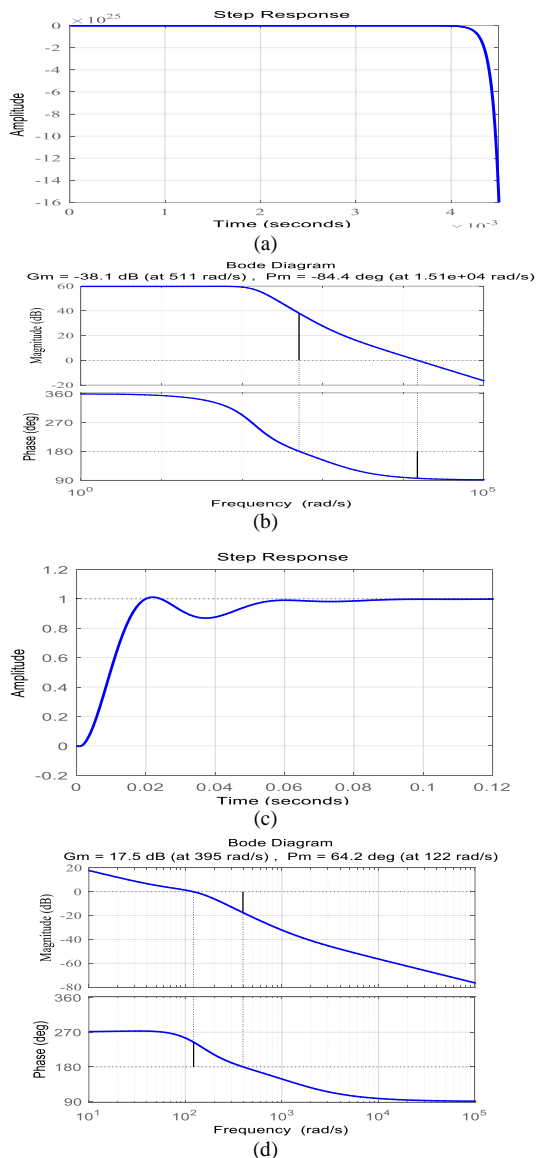

Fig. 14. Results of DC side controller design for the first method, a. Closed-loop step response before design, b. Open-loop bode diagram before design, c. Step response after design, b. open-loop bode diagram after design
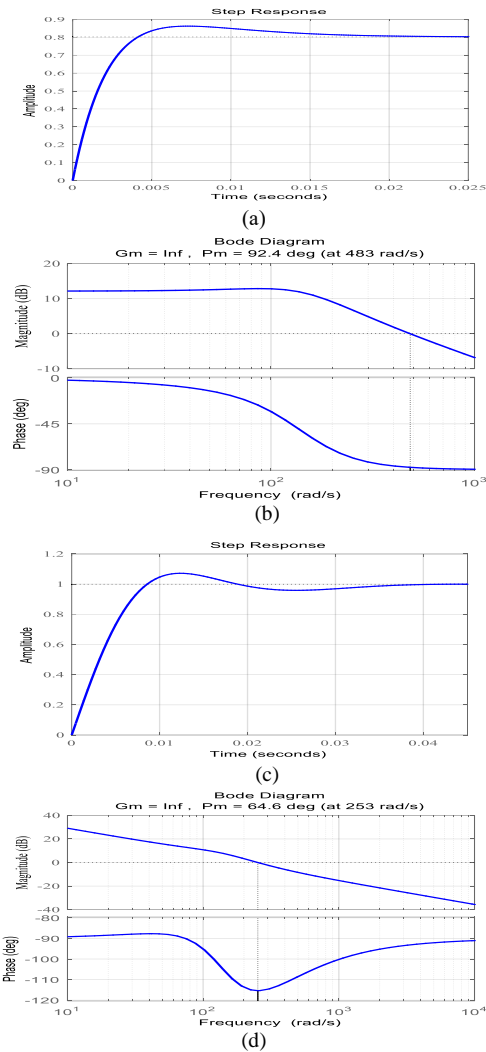

Fig. 15. Results of capacitor voltage control of AC side controller design, a. Closed-loop step response before design, b. Open-loop bode diagram before design, c. Step response after design, b. open-loop bode diagram after design

PV panels are exposed to weather condition changes, so the control system should maintain system stability during irradiance and temperature changes. Irradiance changes have more impact on PV power changes. For this reason, the impacts of irradiance changes are considered in this paper. The P-V characteristic of a photovoltaic array for different amounts of radiation (1000 W/m² and 800 W/m² according to the PV array datasheet) is shown in Fig. 16. The simulation results for both DC side control methods are almost the same. Therefore, the results of the first method are utilized. Fig. 17-a displays the power drop at t = 0.4 s to t = 0.6 s, which is due to changes in the amount of irradiance from 1000 W/m² to 800 W/m². According to Fig.17-b, it can be shown that the MPPT section tracks the maximum power point well and the sinusoidal grid current remains. Therefore, it can be concluded that the control system works well and is stable against irradiance changes.
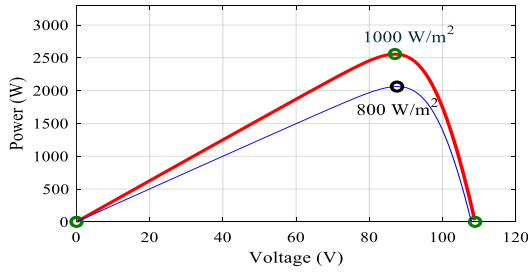
Fig. 16. Solar panel P-V curve by altering irradiance

(a)

(b)
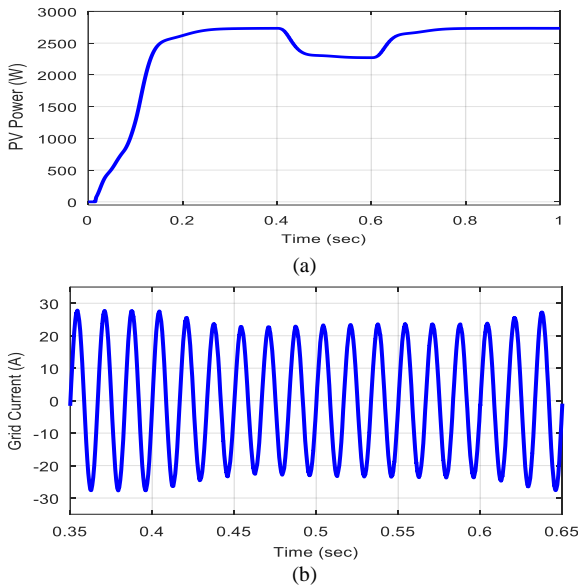
Fig. 17. Response of the system to irradiance change from 1000 W/m² to 800 W/m², a. PV output power, b. Grid current

In order to properly inject the output power of the PV array into the grid, the capacitor voltage is measured and the appropriate control is designed and applied. As can be seen in Fig.18-a, the capacitor voltage ripple is negligible. Even by applying perturbation to change the radiation of the PV array in a time interval of 0.4 to 0.6 seconds, the capacitor voltage control works properly and the capacitor voltage is within the allowable range, and kept close to the reference voltage of the capacitor. Fig. 18-b shows the continuous current of the input inductor, which also decreased due to the reduction of the PV array output power in a period of 0.4 to 0.6

seconds. In the following figures, variation of grid side inductance in the period t = 0.595s to t = 0.705s are investigated. The value of grid side inductor has changed from 175 µH to 875 µH. This change is applied in the worst case, which coincides with the peak of the grid current. Figure 19 shows the grid current when the grid side inductance increases and then decreases suddenly as a worst case. The THD in this case has resulted equal to 1.19%. In this case, the system maintains its stability and the control section of the system works well against variation of grid side inductance.


(a)

(b)
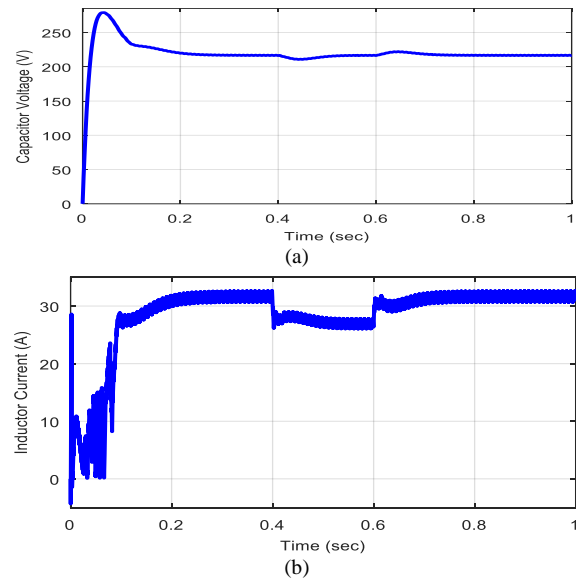
**Fig. 18. a. Capacitor C_1 voltage of QZS network, b. The inductance L_1 current of QZS network**
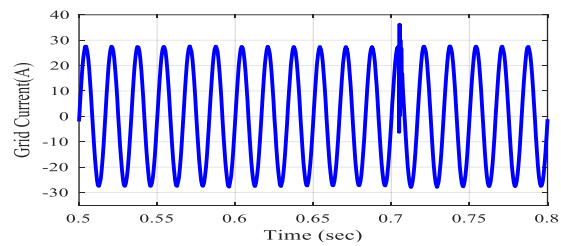
Fig. 19. Grid current during a sudden increasing and decreasing in the grid side inductance

Table 3. Comparison of proposed system with other similar researches

Compared parameters	Grid-connected voltage source converter [23]	Grid-connected PV system [24]	Grid-connected boost inverter [25]	Grid-connected PV inverter [5]	Grid-connected PV inverter [22]	Grid-connected PV inverter [4]	Grid-connected converter [18]	proposed
Converter type	VSC	Trans-Z-Source	Boost Inverter	Trans-Z-Source	Modified-Y-Source	Quasi-Z-Source	Quasi-Z-Source	Quasi-Z-Source
Output filter	LCL with Multi-tuned traps filter	L	L	LCL	LCL	L	L	LCL
AC side controller (coefficient selection)	PI (Design)	PR (Design)	State Feedback Control (Design)	PR (Design)	PR (Design)	PIS (trial and error)	PI (small-signal)	PR (Design)
Capacitor voltage control of AC side (coefficient selection)	✗	PI (trial and error)	✗	PI (trial and error)	PI (trial and error)	PI (trial and error)	P (small-signal)	PI (small-signal)
DC side controller (coefficient selection)	✗	✗	✗	✗	✗	✗	PI (small-signal)	PI (small-signal)
THD%	2.5	2.9	4.52	1.24	1.61	3.62	1.67	1
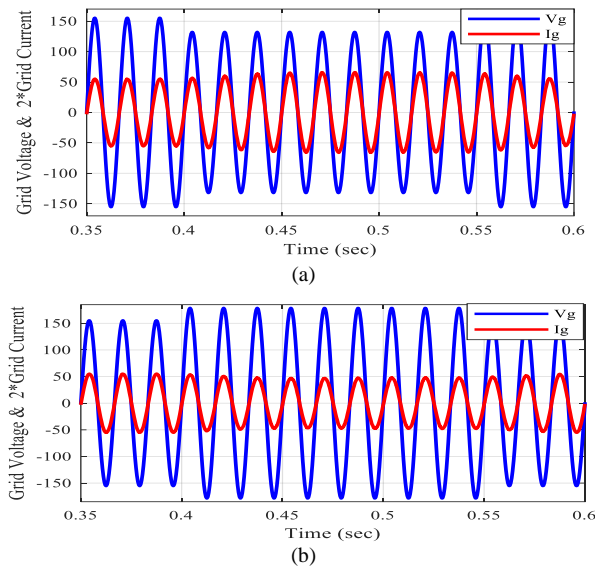
Fig. 20.a. Grid voltage and current with during voltage sag, b. Grid voltage and current during voltage swell

Distributed power generation systems may be exposed to grid voltage fluctuations, in which case the system must maintain its stability. following figures show changes in grid voltage between t = 0.4s and t = 0.55s. Figure 20-a shows the grid voltage and current with a 15% sag in the grid voltage and Figure 20-b shows grid voltage and current with a 15% swell in the grid voltage. The current THD in both aforementioned cases have resulted equal to 1.01%. In both cases, the system maintains its stability and system control section works well against grid voltage changes.

5.1. Comparison with simulation results of similar works

The comparisons between reviewed similar systems and presented method are given in Table 3. Various structures of inverters based on quasi-Z-source converter are connected to the grid with L or LCL filters. In this research, the control system samples the grid current and voltage of the capacitor. To ensure the unit power factor, a PLL block is used to synchronize the injected current with the grid voltage and MPPT is performed for them. The differences between these systems are in the output filter and the control method used on the DC side and the AC side. In the proposed method, an LCL filter is used. The active damping with the PR controller leads to accurate and high-quality injection of power into the grid. THD of the grid current is 1.01%, while in systems with L and LCL filters, THD values have been greater than the value obtained in this paper. It is due to different types of converters and control methods and selection of parameters.

6. CONCLUSION

Due to the development of grid-connected PV-based inverters as Distributed Power Generators, the control of injected power to the grid becomes more important. In this work, a control scheme for a PV based quasi-Z-source inverter which is connected to the grid through an LCL filter is proposed. A two-stage control method is proposed for DC side control to increase the voltage and for AC side control to DC-AC conversion. In the DC side control and capacitor voltage control of the AC side, the PI controller parameters are systematically obtained using the transfer functions, which are extracted from the small-signal analysis. To eliminate the switching harmonics, the converter is connected to the grid via an LCL filter. To control the AC side of the inverter, a grid-connected quasi-Z-source is provided with a systematic method for designing PR control parameters and capacitor current feedback coefficient. The applied two-stage control method can maintain accurate tracking of photovoltaic array power, to inject current into the grid with very good quality and low THD. The simulation results are presented by applying changes in the amount of PV array radiation to analyze the system performance in different conditions.

REFERENCES

[1] H. Yousefi, S. Gholamian and A. Zakariazadeh, "Distributed voltage control in distribution networks with high penetration of photovoltaic systems", *J. Oper. Autom. Power Eng.*, vol. 8, pp. 164-71, 2020.

[2] R. Aghaie and M. Farshad, "Maximum power point tracker for photovoltaic systems based on moth-flame optimization considering partial shading conditions", *J. Oper. Autom. Power Eng.*, vol. 7, pp. 176-186, 2019.

[3] H. Abu-Rub et al., "Quasi-Z-source inverter-based photovoltaic generation system with maximum power tracking control using ANFIS", *IEEE Trans. Sustain. Energy*, vol. 4, pp. 11-20, 2013.

[4] M. Shahparasti et al., "Quasi Z-source inverter for photovoltaic system connected to single phase AC grid", *1st Power Electron. Drive Syst. Technol. Conf.*, pp. 456-460, 2010.

[5] M. Hosseinpour and N. Rasekh, "A Single-Phase Grid-tied PV based Trans-Z-Source Inverter Utilizing LCL filter and Grid Side Current Active Damping", *J. Energy Manage. Technol.*, vol. 3, pp. 67-77, 2019.

[6] M. Farhadi Kangarlu, E. Babaei and F. Blaabjerg, "An LCL-filtered single-phase multilevel inverter for grid integration of PV systems", *J. Oper. Autom. Power Eng.*, vol. 4, pp. 54-65, 2016.

[7] P. Alemi, C. Bae and D. Lee, "Resonance suppression based on PR control for single-phase grid-connected inverters with LLCL filters", *IEEE J. Emerg. Selected Top. Power Electron.*, vol. 4, pp. 459-467, 2015.

[8] S. Jayalath and M. Hanif, "An LCL-filter design with optimum total inductance and capacitance", *IEEE Trans. Power Electron.*, vol. 33, pp. 6687-98, 2017.

[9] W. Wu et al., "Damping methods for resonances caused by LCL-filter-based current-controlled grid-tied power inverters: an overview", *IEEE Trans. Ind. Electron.*, vol. 64, pp. 7402-13, 2017.

[10] R. Alzola et al., "Analysis of the passive damping losses

in LCL-filter-based grid converters", *IEEE Trans. Power Electron.*, vol. 28, pp. 2642-46, 2012.

[11] B, Bahrani, M. Vasiladiotis and A. Rufer, "High-order vector control of grid-connected voltage-source converters with LCL-filters", *IEEE Trans. Ind. Electron.*, vol. 61, pp. 2767-75, 2013.

[12] X. Wang, F. Blaabjerg and P. Loh, "Grid-current-feedback active damping for LCL resonance in grid-connected voltage-source converters", *IEEE Trans. Power Electron.*, vol. 31, pp. 213-23, 2015.

[13] N. Rasekh et al., "A step by step design procedure of PR controller and capacitor current feedback active damping for a LCL-type grid-tied T-type inverter", *Int. Power Electron. Drive Syst. Technol. Conf.*, pp. 612-617, 2019.

[14] Z. Xin et al., "Highly accurate derivatives for LCL-filtered grid converter with capacitor voltage active damping", *IEEE Trans. Power Electron.*, vol. 31, pp. 3612-25, 2015.

[15] X. Wang, F. Blaabjerg and P. Loh, "Grid-current-feedback active damping for LCL resonance in grid-connected voltage-source converters", *IEEE Trans. Power Electron.*, vol. 31, pp. 213-23, 2015.

[16] Y. Guan et al., "The dual-current control strategy of grid-connected inverter with LCL filter", *IEEE Trans. Power Electron.*, vol. 34, pp. 5940-52, 2018.

[17] M. Forouzesh et al., "Small-signal modeling and comprehensive analysis of magnetically coupled impedance-source converters", *IEEE Trans. Power Electron.*, vol. 31, pp. 7621-7641, 2016.

[18] Y. Li et al., "Modeling and control of quasi-Z-source inverter for distributed generation applications", *IEEE Trans. Ind. Electron.*, vol. 60, pp. 1532-54, 2012.

[19] A. Ayad and R. Kennel, "A comparison of quasi-Z-source inverters and conventional two-stage inverters for PV applications", *EPEJ,* vol. 27, pp. 43-59, 2017.

[20] Y. Liu et al., "Modelling and controller design of quasi-Z-source inverter with battery-based photovoltaic power system", *IET Power Electron.*, vol. 7, pp. 1665-74, 2014.

[21] N. Rasekh et al., "Robust power conditioning system based on LCL-type quasi-Y-source inverter for grid connection of photovoltaic arrays", *Int. J. Autom. Control*, 2021.

[22] N. Rasekh and M. Hosseinpour, "Adequate tuning of LCL filter for robust performance of converter side current feedback control of grid connected modified–y-source inverter", *Int. J. Ind. Electron. Control Optimiz.,* vol. 3, pp. 365-378, 2020.

[23] M. Sanatkar-Chayjani and M. Monfared, "Stability analysis and robust design of LCL with multituned traps filter for grid-connected converters", *IEEE Trans. Ind. Electron.*, vol. 63, pp. 6823-34, 2016.

[24] A. Rajabi, M. Simab and J. Aghaei, "Design of a power-conditioning system for trans-z-source inverter to connect photovoltaic arrays to single-phase household electrical grid", *Iran. J. Sci. Technol. Trans. Electr. Eng.*, vol. 42, pp. 393-402, 2018.

[25] N. Noroozi and H. Gholizade Narm, "Direct power control of an under-damped grid connected boost inverter", *Int. J. Ind. Electron. Control Optimiz.*, vol. 2, pp. 17-24, 2019.

[26] M. Hosseinpour and A. Dejamkhooy, "Control and power sharing among parallel three-phase three-wire and three-phase four-wire inverters in the presence of unbalanced and harmonic loads", *IEEJ Trans. Electr. Electron. Eng.*, vol. 13, pp. 1027-33, 2018.

[27] C. Bao et al., "Step-by-step controller design for LCL-type grid-connected inverter with capacitor–current-feedback active-damping", *IEEE Trans. Power Electron.*, vol. 29, pp. 1239-53, 2013.